Hybrid Optical Switch Using Passive Polymer Waveguides and Semiconductor Optical Amplifiers

Regis S. Fan and R. Brian Hooker

***Abstract*—Optical switching can be performed by using optical amplifiers combined with a passive waveguiding network. Recently, most of the effort in optical amplifier switch modules have been focused on monolithic switches in which the entire device is fabricated on an InP substrate together with the semiconductor optical amplifiers (SOA's). In this paper, we investigate the use of SOA's with passive polymer waveguides to make hybrid switches of varying sizes. The optical amplifiers serve dual purposes, gating the signal and amplifying the signal. Amplification is needed in order to offset the losses associated with the passive waveguide elements as well as the losses from component misalignments in the switch module. Our analysis finds the largest switch module size that can be made with the architecture used. We also calculate the maximum number of switch modules which can be cascaded in order to retain a bit-error rate (BER) under 10^{-9}.**

***Index Terms*—Hybrid optical switch, optical switch, polymer waveguides, semiconductor optical amplifier (SOA) switch.**

I. Introduction

OPTICAL switching has been a major area of interest since the advent of optical communication systems. There are several different types of optical switches including mechanical, directional coupler, Mach–Zehnder, and optical amplifier switches. Mechanical switches suffer from relatively slow switching speeds. It is difficult to obtain high extinction ratios with directional coupler and Mach–Zehnder switches, which can lead to unwanted crosstalk. Recently, there has been much attention to optical amplifier switches since they have large extinction ratios and also have the ability to amplify the signal to offset the losses which are present.

There have been many researchers who have looked into making switches with optical amplifiers, as long ago as the early 1980's [1], [2]. Since then, most optical switches using SOA's have focused on making a monolithic switch in the same material containing the SOA. This approach can help alleviate the misalignment between the passive waveguide routing part of the device and the amplifiers, however these devices often require complicated multistep epitaxial growth and complex processing [3]. There have been devices made at wavelengths of both 1.3 and 1.55 μm. Several different 2×2 monolithic SOA switches which have been made at AT&T Bell Labs [4], France Telecom [5], British Telecom [6], Ericsson Components [7], the Institute of Quantum Electronics, Zurich, Switzerland [8], NEC Corporation [9], and the Electronics and Telecommunications Institute, Taejon, Korea [10]. There have also been 4×4 switches made by Ericsson Components [11], [12]. A hybrid technique for making a 4×4 optical switch using silica-based optical waveguides and SOA's [13] was described by NTT Opto-electronics Laboratories.

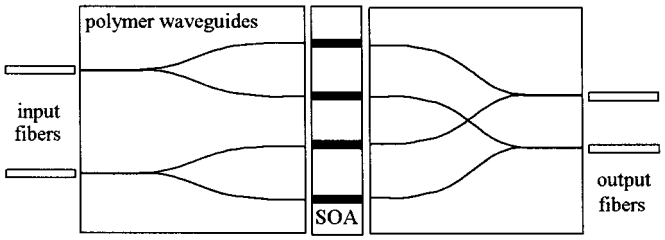

Fig. 1. 2×2 hybrid SOA switch module.

There have been many studies on lightwave systems using optical amplifiers, including switches. The propagation of amplified spontaneous emission (ASE) noise through lightwave systems has been studied by several researchers [14]–[18]. The effect of residual reflectivity on the SOA end facets has been analyzed [19]. The reflections between the waveguide and the SOA's were also investigated, and seen to be a large factor in a hybrid optical switch using silica-based waveguides [13]. In other studies, the crosstalk implications in optical networks have been analyzed and are shown to effect the signal-to-noise ratio (SNR) of optical systems [20], [21]. The impact of the input signal power on SOA switch systems have been investigated [22]. Effects of the input polarization state on SOA-based switches was also studied [23]. In this paper, we take these studies one step further and perform a more intensive investigation of an switch using a passive polymer waveguide network. The comprehensive analysis of the losses in the passive polymer waveguide network, including the effects of misalignments, is done using a Monte Carlo technique.

The structure for the optical switch under investigation is shown in Figs. 1 and 2. It is shown for a 2×2 and a 4×4 switch. Larger switches can also be designed using the same type of architecture which is called a Matrix Vector Multiplier (MVM) switch [14], [20]. In these switches there is only one SOA which is traversed for any branch of the switch. Thus, this single SOA is used for gating as well as for amplifying the signal to counter losses in the entire switch module.

In this paper, we describe the work involved with the design of an integrated optical switch using semiconductor optical amplifiers (SOA's) and passive polymer waveguides. In Section II, we look at the module design and alignment techniques which includes a Monte Carlo analysis which shows the effect of the misalignment of the different components in the module. In

Manuscript received April 15, 1999; revised October 18, 1999. This work was supported in part by Astarté Fiber Networks, Inc.

The authors are with the Department of Electrical Engineering, University of Colorado at Boulder, Boulder, CO 80309 USA.

Publisher Item Identifier S 0733-8724(00)03030-9.

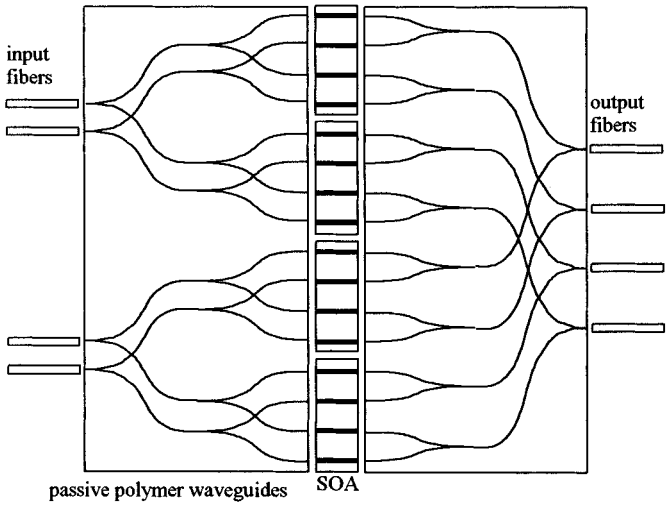

Fig. 2. 4×4 hybrid SOA switch module.

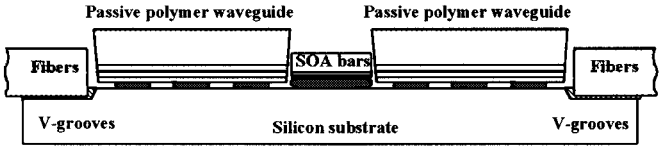

Fig. 3. Configuration 1. Flip-Chip attachment of three elements.

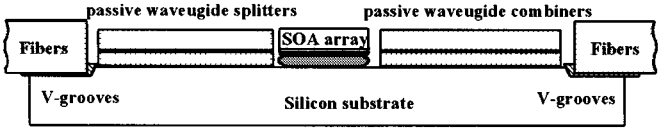

Fig. 4. Configuration 2. Flip-chip attachment of SOA's on substrate containing passive polymer waveguides.

Section III, we look into the maximum switch array size, taking into account the BER and gain saturation of the SOA's. We also find the maximum number of stages which can be cascaded, in order to find the switching array size that can be made using the smaller switch modules as building blocks.

II. Coupling Losses and Module Design

In this section, we analyze the coupling losses in the entire switch module for the two different configurations shown in Figs. 3 and 4. In configuration 1, both the waveguides and SOA's are flip-chip bonded onto the substrate. In configuration 2, the waveguides are fabricated directly onto the substrate, and thus the waveguides can be photolithographically defined, and aligned, with respect to the V-grooves and the flip-chip bond pad metallization.

In order to determine the coupling efficiency of the entire switch module a Monte Carlo analysis was performed. We assume that the component placement has a misalignment with a Gaussian distribution. The Gaussian distribution is defined by

$$f(x) = \frac{1}{\sqrt{2\pi}\sigma} \exp\left(\frac{-x^2}{\sigma^2}\right). \tag{1}$$

We assume that the misalignment tolerance corresponds to the 2σ value of the Gaussian distribution. The 2σ tolerance value

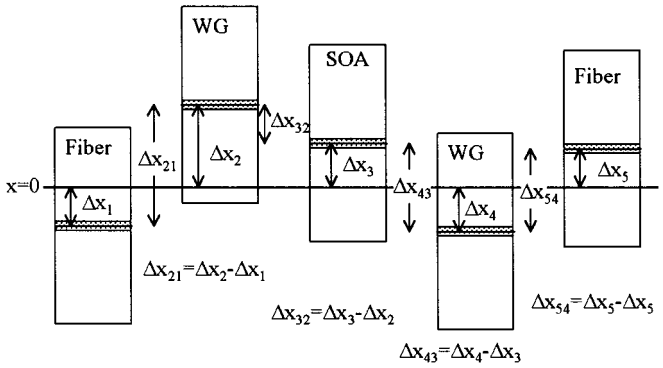

Fig. 5. Misalignments of components in the hybrid switch for configuration 1.

implies that there are 95.5% of the devices with a misalignment within the tolerance value.

For all of the misalignments, the offset between components is calculated by keeping track of the previous misalignment, since the misalignments are not independent of each other. Fig. 5 shows how the misalignments are related, and how they are calculated for the x and y directions. As can be seen, there are five different components (two fibers, two waveguides, and one SOA) which need to be combined onto the substrate, all of which have misalignments associated with them. What is important is the offsets between the respective components. The offsets are calculated by taking the difference between the two adjacent components. The individual component misalignments are found from randomly generated numbers whose elements are normally distributed with mean 0 and 2σ value equal to the alignment tolerance. As can be seen in Fig. 5, the individual misalignments are calculated with respect to the optical axis which corresponds to the line labeled $x = 0$.

In the z direction, the component separations is calculated in a similar way. In this case, the separation between the first and second components is

$$\Delta z_{21} = \mathrm{sep}_{21} + \Delta z_2 - \Delta z_1 \tag{2}$$

where sep_{21} is the nominal separation between the two components, and Δz_1 and Δz_2 are the misalignments of the respective components. The separations between the subsequent components are calculated in the same way.

The Monte Carlo analysis was run for 10 000 cases of randomly generated offsets for each individual component. The coupling efficiencies were then calculated between all of the individual components and were combined to get the overall coupling efficiency for the entire module. The coupling loss thus includes both the mode mismatch loss and the misalignment loss. In order to reduce computation time, the coupling efficiencies were first calculated between all of the components over a 3-dimensional grid.

The coupling efficiencies between all of the components were calculated for z separations between 0 and 10 μm with a sample spacing of 0.2 μm. The spot size of the fiber is circular with a diameter of about 10 μm. The spot size of the SOA is elliptical with dimensions of approximately 1×3 μm. The waveguide structure contains a taper structure which was optimized

TABLE I
PARAMETERS FOR MONTE CARLO COUPLING ANALYSIS

Parameter	Value
x tolerance ($2\sigma_x$)	2 μm
y tolerance ($2\sigma_x$)	1 μm
z tolerance ($2\sigma_x$)	2 μm
nominal waveguide to fiber separation	5 μm
nominal waveguide to SOA separation	5 μm

for coupling between the SOA and fiber [24]. In order to calculate the coupling efficiencies, the near field mode profiles of the individual components were used. The mode of the output device was first propagated from the output device to the input device (e.g., fiber-to-waveguide or waveguide-to-SOA, etc.) using a Rayleigh-Sommerfeld free space beam propagation program [25]. Next, an overlap integral was used to calculate the coupling efficiency between the components.

The efficiencies were calculated in the x (lateral) direction from -6.5 to 6.5 μm with a sampling space of $\lambda/8$ (0.1625 μm), and y (vertical) direction from -3.25 to 3.25 μm, also with a sampling space of $\lambda/8$. Thus there were 160 000 coupling efficiencies that were calculated and stored in a 3-dimensional array for each of the component pairs (fiber-to-waveguide, waveguide-to-SOA, SOA-to-waveguide, and waveguide-to-fiber). The coupling efficiencies for a given misalignment was then found by accessing the corresponding element of the array. With this technique the coupling efficiencies had to be calculated only once instead of multiple times during the Monte Carlo analysis, saving significant computation time. Since the Rayleigh-Sommerfeld propagation is the most computationally expensive step, the field was propagated to one plane, and then all of the coupling efficiencies for that plane were calculated.

A. Monte Carlo Coupling Results

The following misalignment tolerances were used for all of the components in the Monte Carlo analysis of coupling efficiencies for configuration 1 are shown in Table I, and correspond to the alignments that can be achieved using a passive flip-chip bonding process.

The Monte Carlo analysis was also run for the second configuration which has the waveguides made directly on the substrate. The offsets in the x and y directions are the same as in configuration 1, but with the misalignments of the waveguide sections set to zero. Thus $\Delta x_2, \Delta y_2, \Delta x_4, \Delta y_4$ are all assumed to be zero since the waveguides are photolithographically defined directly on the substrate. There is a slight difference in the component separations compared to configuration 1, since there is now a different relationship among the separations between the first waveguide section and the SOA's, and between the SOA and second waveguide section. The sum of those two separations is constant (the SOA is placed in a gap between the two waveguide sections). We assume a total gap between SOA and waveguide sections of 10 μm (sum of the waveguide to SOA separation and SOA to waveguide separation). We use the same values for the x, y, and z tolerances $(2\sigma_x = 2, 2\sigma_y = 1, 2\sigma_z = 2)$ as for configuration 1, and again assume a waveguide to fiber nominal separation of 5 μm.

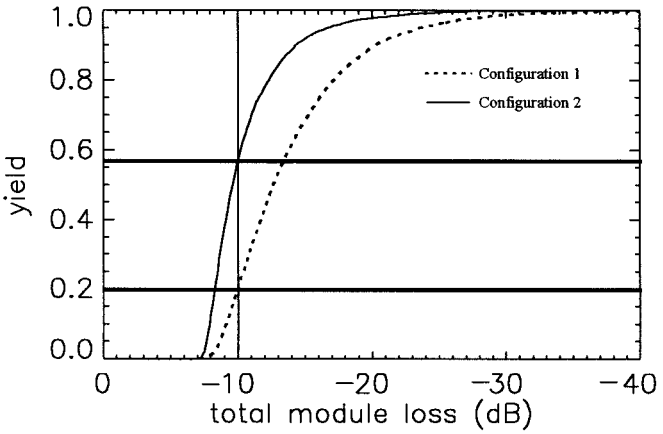

Fig. 6. Yield versus module loss for configuration 2 and configuration 1.

The coupling losses were calculated for the entire module, keeping track of the losses before and after the SOA. The minimum pre SOA loss was found to be -3.09 dB, and the minimum post SOA loss was -2.95 dB. In Fig. 6, we can see the yield versus total module loss of the entire module for both configurations. The minimum total module loss was found to be -6.78 dB, so the yield is 0% for losses less than -6.78 dB. We can see that for configuration 1 there is a yield of about 20% for a module loss of -10 dB.

As can be seen by comparing with the results from coupling losses for configuration 1, the losses are lower for configuration 2. For example in configuration 2, the yield is about 60% for a module loss of -10 dB, compared to the 20% yield seen for configuration 1. The coupling losses are lower since the waveguide sections are fabricated directly on the substrate, and thus the misalignments lessened. The minimum pre-SOA, post-SOA and total loss were found to be the same as for configuration 1. This is expected, since these values correspond to a case where all of the components have minimal misalignments. The difference is that the 'best case' occurs more frequently in configuration 2, which manifests itself in the higher yield. Since the coupling losses are lower for configuration 2, we conclude that configuration 2 is the more desirable of the two configurations, although the fabrication is perhaps more difficult. Configuration 2 requires etching of the waveguide channels to make the gap for the placement of the SOA array.

III. SWITCH ARRAY SIZE

In order to determine a reasonable individual switch module array size, there are several things that must be considered. We must first find the entire loss through the module. The entire module loss is calculated, including the coupling losses from the previous section, and losses in the passive polymer waveguide network. We then find the maximum number of 2×2 and 4×4 switch module stages that can be cascaded. The maximum number of 2×2 stages allows us to find the size of a switch network that can be built using the 2×2 switch module as a building block to make a larger network.

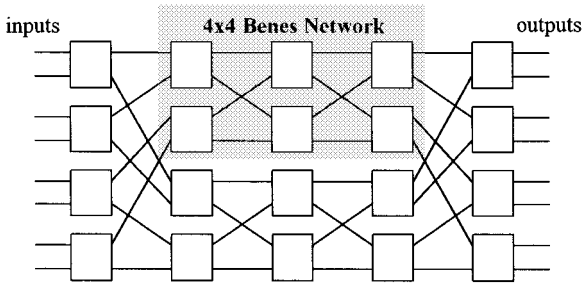

Fig. 7. Benes network.

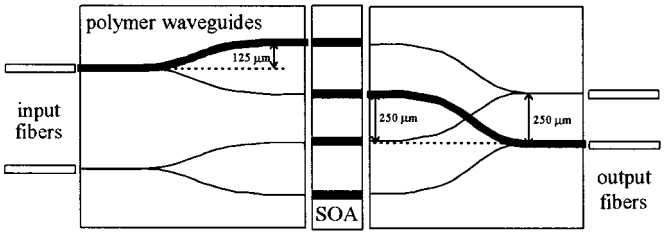

Fig. 8. 2×2 switch module showing channel separations and worst case channel pathway.

TABLE II
SUMMARY OF 2×2 WAVEGUIDE LOSSES

	Loss mechanism	Loss (dB)
pre SOA loss	S-bend loss (125 μm translation)	-0.155
	Splitter loss	-3.1
	Channel crossing	0
	Channel loss	-0.0992
	Total pre SOA loss	**-3.3542**
post SOA loss	S-bend loss (250 μm translation)	-0.2175
	Combiner loss	-3.1
	Channel crossing (40.7° angle)	-0.057054
	Channel loss	-0.1392
	Total pre SOA loss	**-3.54406**

A. Larger Switch Network Using 2×2 Switch Module as a Building Block

We can make a larger switching network using a smaller switch module as a building block. An example of such a large network is shown in Fig. 7. This network is called the Benes network and is made up of 2×2 switch modules. The Benes network is rearrangeably nonblocking and uses $2 \cdot \log_2 N - 1$ stages, with $N/2$ switches per stage, for an $N \times N$ switch [26]. For example, a 128×128 Benes network needs 13 stages and a 4096×4096 needs 23 stages.

B. Total Switch Module Loss

In calculating the losses in the waveguide sections, we looked at the channels with the most loss (worst case). In Fig. 8, the channels analyzed are shown in bold for the 2×2 switch module, which contains one channel crossing in the waveguide section after the SOA. The waveguide losses include splitter loss, channel bends, channel crossings. Table II shows a summary of the losses for the waveguide sections. The channel bends were designed to have a radius of curvature of 2000 μm.

The same loss analysis was performed for the 4×4 switch module for the worst case channel shown in bold in Fig. 9. We

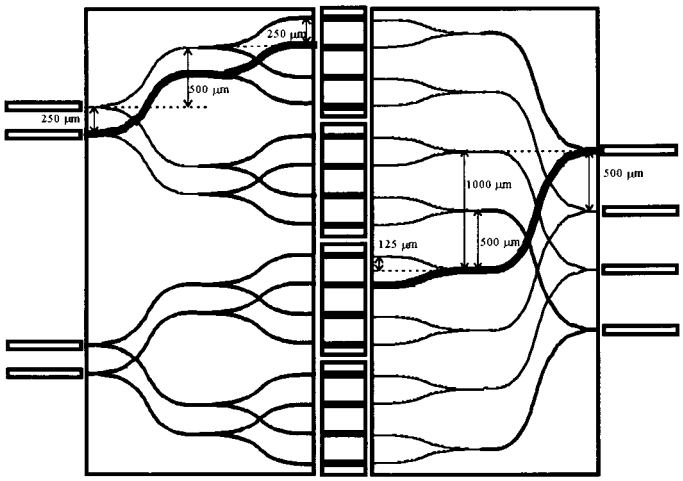

Fig. 9. 4×4 switch module showing channel separations and worst case channel pathway.

TABLE III
SUMMARY OF 4×4 WAVEGUIDE LOSSES

	Loss mechanism	Loss (dB)
pre SOA loss	S-bend loss (500 μm translation)	-0.3025
	Splitter loss	-3.1
	Channel crossing 1 (40.7° angle)	-0.057054
	S-bend loss (250 μm translation)	-0.2175
	Splitter loss	-3.1
	Channel crossing 2 (40.7° angle)	-0.057054
	Channel loss	-0.3328
	Total pre SOA loss	**-7.167**
post SOA loss	S-bend loss (125 μm translation)	-0.155
	Combiner loss	-3.1
	Channel crossing 1 (57.9° angle)	-0.040606
	Channel crossing 2 (82.8° angle)	-0.033185
	Channel crossing 3 (57.9° angle)	-0.040606
	S-bend loss (1000 μm translation)	-0.41344
	Combiner loss	-3.1
	Channel loss	-0.3638
	Total pre SOA loss	**-7.247**

can see that the worst case pre-SOA channel has two-channel crossings, and the worst case post-SOA channel contains three-channel crossings, at two different angles. The total loss for the 4×4 module is summarized in Table III.

We can now combine the waveguide loss together with the coupling losses between the different components (Monte Carlo analysis) to get the total module loss which includes channel loss, bend loss, channel crossing, splitter loss, and combiner loss and coupling losses. In Fig. 10, we can see the total module loss as a function of the yield for the two module attachment configurations. For both configurations, the total loss increases as the yield increases. By observing the losses for the two configurations, we see that configuration 2 produces lower overall loss in the module, due to better coupling characteristics. There is about a 2-dB difference in the module loss for a 20% yield, increasing to about a 4-dB difference in loss for the 80% yields.

If we assume a maximum SOA gain of 28 dB, we can see that the gain can overcome the losses for all of the 2×2 module yields, and most of the 4×4 switch module yields. For an 8×8 switch, however, there would be an additional loss of at least 6.2 dB due to an additional splitter and combiner, making the

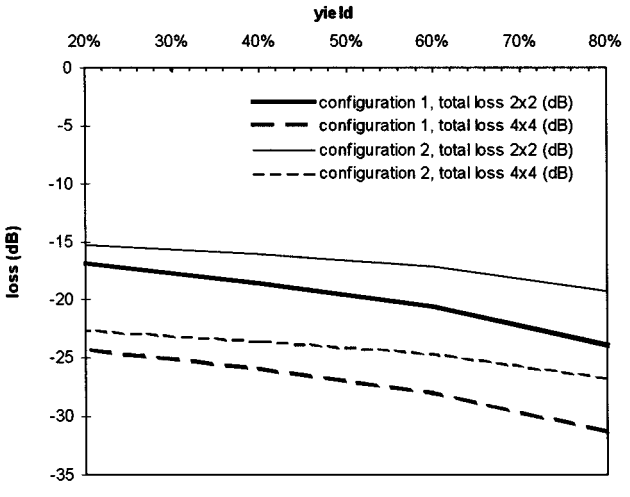

Fig. 10. Total module loss including waveguide losses and coupling losses.

loss difficult to overcome. We therefore center our attention on a maximum switch module size of 4×4.

C. Noise and Bit-Error Rate (BER)

There are several noise contributors in the switch including signal extinction ratio and amplifier noise. Channel crosstalk, especially coherent crosstalk, is another source which can degrade the signal-to-noise ratio (SNR), but is not considered in this study. In general the amplifier noise, or amplified stimulated emission (ASE), dominates over the other noise mechanisms in most SOA switch systems. The ASE power is given by

$$P_{\rm sp} = p \cdot S_{\rm sp} \cdot \Delta\nu_{\rm sp} \tag{3}$$

where $\Delta\nu_{\rm sp}$ is the effective band width of the spontaneous emission and p is the number of modes which is two for a polarization insensitive amplifier [transverse electric (TE) and transverse magnetic (TM)]. $S_{\rm sp}$ is the spectral density of the spontaneous emission given by

$$S_{\rm sp} = n_{\rm sp}(G-1)h\nu. \tag{4}$$

And $n_{\rm sp}$ is the amplifier population-inversion parameter. A complete list of the parameters can be seen in Table IV.

The ASE manifests itself in the form of beating terms with the signal, with itself and with the shot noise in the detector. These three noise terms are the signal-spontaneous beating [27]

$$\sigma^2_{\rm sig-sp} = 4R^2GP_sS_{\rm sp}\Delta f \tag{5}$$

and the spontaneous–spontaneous beating[1]

$$\sigma^2_{\rm sp-sp} = 4R^2S^2_{\rm sp}\Delta\nu_{\rm opt}\Delta f. \tag{6}$$

There is also the shot noise

$$\sigma^2_s = 2q(R(GP_s + P_{\rm sp}) + I_d)\Delta f \tag{7}$$

[1]There are inconsistencies in the equation for the spontaneous-spontaneous beating noise, either using a factor of 2 or a factor of 4 in this equation [15], [27]. We use the factor of 4 since it corresponds to a larger noise, and thus a worst case scenario.

TABLE IV
PARAMETER LIST

Parameter List	
Δf	Electrical bandwidth
$\Delta\nu_{sp}$	Spontaneous emission bandwidth
$\Delta\nu_{opt}$	Optical filter bandwidth
R	Receiver responsivity ($\eta q/h\nu$)
η	Quantum efficiency of detector
q	Electron charge
$h\nu$	Photon energy
p	Number of modes
G	Amplifier gain
S_{sp}	Spontaneous emission spectral density
P_{sp}	Spontaneous emission power
P_s	Signal power
n_{sp}	Population-inversion parameter
I_d	Detector dark current
k_B	Boltzmann constant
T	Temperature (K)
R_L	Load resistor
I_1	Signal current for a "1" bit
I_0	Signal current for a "0" bit
σ_1	Noise current for a "1" bit
σ_0	Noise current for a "0" bit

and the thermal noise in the detector

$$\sigma^2_T = \frac{4k_BT}{R_L}\Delta f. \tag{8}$$

The total noise current contribution is

$$\sigma^2_{\rm total} = \sigma^2_{\rm sig-sp} + \sigma^2_{\rm sp-sp} + \sigma^2_s + \sigma^2_T. \tag{9}$$

In order to design a system, there needs to be a design criteria. One such criteria that can be used the BER which is determined by [28]

$$\text{BER} = \frac{1}{2}\,\text{erfc}\left(\frac{Q}{\sqrt{2}}\right) \tag{10}$$

where erfc is the complementary error function and

$$Q = \frac{I_1 - I_0}{\sigma_1 + \sigma_0}. \tag{11}$$

D. Maximum Number of Switch Module Stages

sIn order to determine the maximum number of switches which can be cascaded in order to form a larger switching network, we calculated the BER through multiple stages of the hybrid switches using the model described in Section III-C. Fig. 11 illustrates a cascaded switch system of N cascaded stages. For the ASE calculation and propagation, the spontaneous emission bandwidth $(\Delta v_{\rm sp})$ is used to calculate the spontaneous emission power which propagates through the system of N stages until it reaches the optical filter $(\Delta v_{\rm opt})$ placed before the detector. The thermal noise in the detector is calculated with a temperature of 300 K. In calculating the maximum number of cascadable stages of 2×2 and 4×4 stages, we require that the BER remain below a value of 10^{-9}.

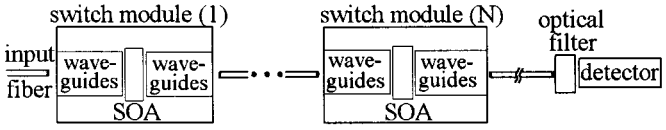

Fig. 11. N cascaded stages of optical switch modules.

An optical filter bandwidth of 1 nm was used. The analysis was performed with the amplifier saturating according to

$$G = G_o \exp\left(-\frac{G-1}{G}\frac{P_{\text{out}}}{P_s}\right) \tag{12}$$

where G is the gain, G_o is the unsaturated gain, P_{out} is the output power and P_s is the saturation power.

The SOA's are assumed to be polarization insensitive optical amplifiers operating at a wavelength of 1.3 μm. There are several such amplifiers being developed and some being sold commercially. The other amplifier parameters that were used are $n_{\text{sp}} = 3$, a maximum gain of value of 28 dB, and a saturation output power of $+10$ dBm. The signal coming into the switch was assumed to have an infinite extinction ratio so that the effects of the propagating ASE would be more evident.

As we have seen, there are many sources of loss and only one source of gain, the SOA. A switch (or other device) that has no net loss is also referred to as transparent. Reflections were seen to negatively affect the operation of an optical SOA switch [13], and must be significantly reduced in order to have a good, working switch. In this analysis we assume that the back reflections are sufficiently low that they can be neglected. The total loss from all of the loss mechanisms were combined into two loss parameters per switch module. The first loss parameter includes the losses in the switch module before the SOA, and the second parameter includes the losses after the SOA. This was done since the amplified spontaneous emission (ASE) noise is only affected by the loss after the SOA in the module. The signal power, however, is degraded by the pre-SOA loss as well as the post-SOA loss.

In the two following sections, we analyze the maximum number of switch modules can be traversed for both the 2×2 and 4×4 modules. The distance between the switch modules is assumed to be small so that the loss in the fiber between the switches can be neglected. This is done so that we can see the size of a larger local switch network using the modules as building blocks. The fiber loss can not be neglected if the distance between the switches is large, for example between different switching nodes, since the fiber loss could then become significant.

1) Maximum Number of Cascadable 2×2 Switch Modules: We first analyze the 2×2 switch module, to find the maximum number of cascadable stages. In order to find the maximum number of stages, we performed simulations of the entire module using the losses from Section III-B. There are two different mechanisms that limit the number of stages that can be cascaded. The first the BER, and the second is the amplifier saturation.

In order to see some of the salient features of how many stages can be cascaded, we begin by showing the maximum number of stages of cascaded 2×2 switches for a 40% device yield for configuration 1. As can be seen from Fig. 6, there is a coupling loss of -11.68 dB loss due to misalignment for a 40% yield using configuration 1. From Table II, we can also see that there is -3.354 dB loss in the waveguide section before the SOA and -3.544 dB loss in the waveguide section after the SOA. We calculated the number of stages for varying input powers for 3 cases. The 3 cases were for an equal amount of loss before and after the SOA, the minimum amount of loss before the SOA and the minimum loss after the SOA. This is done because the coupling losses are calculated for the entire module but does not tell us how the loss is distributed before and after the SOA. It is important to know that amount of loss that occurs before and after the SOA, since this will effect the SOA saturation and gain characteristics.

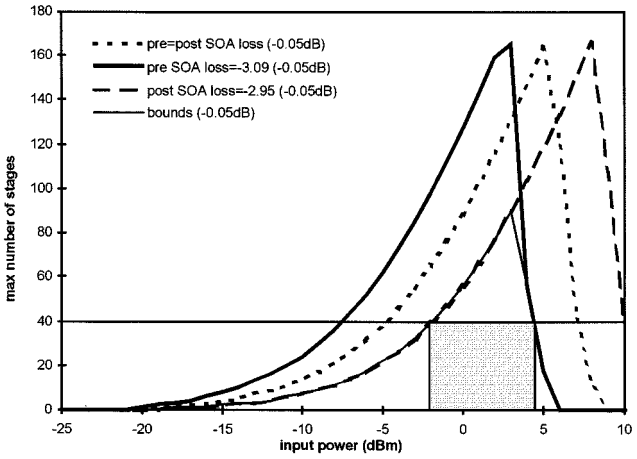

Fig. 12. Maximum number of stages for 40% yield using configuration 1, as a function of the input power to the switch module.

Simulations were run assuming these three different cases, using a BER requirement of 10^{-9}, a bit rate of 10 GHz, and an optical filter bandwidth of 1 nm placed before the detector. Fig. 12 shows the maximum number of stages that can be cascaded as a function of the input power to the switch module. The input power is defined as the power emitted from the inputting fiber, so the power input to the SOA is decreased by the coupling losses and the losses before the SOA in the passive waveguides. Fig. 12 shows the results of the three different cases with a module loss of -0.05 dB. By looking at each of the curves, we can see that the maximum number of stages increases with increasing input power up to a certain point. For this portion of the curve, the maximum number of stages is limited by the BER requirement. Once the input power reaches a certain point, the maximum number of stages begins to decrease. At this point, the maximum number of stages begins to be limited by the amplifier saturation.

We can also observe that the case with the minimum pre SOA loss has a maximum number of stages which occurs for the lowest input power. And the case with the minimum post SOA loss has a maximum number of stages that occurs for the highest input power. The case with the pre SOA and post SOA loss being equal has its peak that occurs between the two extreme cases. In order to be sure that the number of stages is valid for all of the switches with the 40% yield, we use the two extreme cases as the bounds for the number of stages. We then look at the overlap

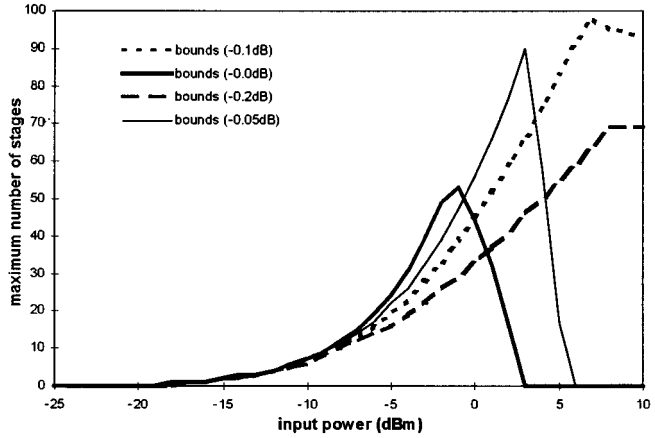

Fig. 13. Maximum number of stages for varying module loss (configuration 1, 40% yield), as a function of the input power to the switch module.

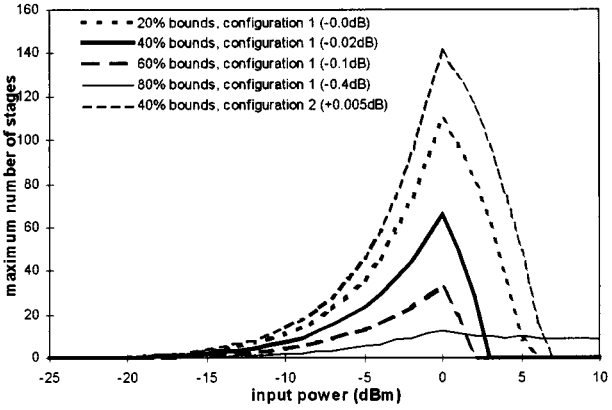

Fig. 14. Maximum number of cascadable 2×2 switch modules for different module yields, as a function of the input power to the switch module.

between the two curves for the extreme cases. This is shown in the graph, labeled as "bounds," and corresponds to the overall maximum number of stages for the switch module with a 40% yield in configuration 1.

If we have a requirement of using a range of input powers, then the maximum number of stages can also be found. For example, as seen from Fig. 12, for a maximum of 40 cascadable stages, there is an input range of about -2 to 4 dBm. This range is shown as the shaded area in the graph.

Fig. 13 shows the maximum number of stages for the 40% yield, using the bounds from the two extreme cases. The are several curves which correspond to different losses through the switch module. The curve for -0.0-dB loss corresponds to a transparent switch, where the gain in the SOA compensates for all of the losses due to the misalignments and waveguide losses. It can be seen that the maximum number of stages occurs for the case where there is actually -0.1-dB loss through the switch module. For the case of the transparent switch, it can be seen that the amplifier saturation begins to take effect for an input power of about -2 dBm. For the case of 0.1-dB loss per amplifier stage, the saturation effects begin for an input power of about 6 dBm. The SOA saturation is more predominant for the case of the transparent switch because the ASE power which is added at each stage continues to grow, whereas the signal power remains constant (the gain at each stage is defined as the gain of the signal). So for the transparent switch, the signal power remains constant, but the ASE grows, thus increasing the total power input to each switch, and the amplifiers begin to saturate sooner. When there is a little bit of loss in each switch module, the signal power decreases slightly, and the ASE still grows, but in this case the total input power (sum of the signal power and ASE power) is lower, and thus the amplifiers saturate for a larger input power.

The overall module gain which is the best for the switch module depends upon the input power. For example, if the input power to the first stage is -2 dBm, then the transparent switch is the best choice, however if the input power to the first switch is 6 dBm, then the switches with a -0.1-dB loss per module becomes the obvious choice.

We now look at the maximum number of stages for different module yields with the results for the 2×2 switch shown in Fig. 14. The maximum number of stages is plotted assuming an input power of 0 dBm for configuration 1 with several yields, and for configuration 2 with a 40% yield. We assumed an input power since the maximum number of stages was seen to be a function of the input power as the module loss varies. By observing the curves for configuration 1 we can see that the maximum number of stages occurs for the 20% yield which has the lowest loss, and the 80% yield has the lowest maximum number of cascadable stages. We can also observe that for the 0 dBm input power, the maximum number of stages occurs for a different total module loss, for the different yields. For the 20% yield, the transparent switch produces the maximum. As the module yield increases, the module loss for the same input power also increases. For example, with the 80% yield, a module loss of -0.4 dB produces the peak maximum number of for the input power of 0 dBm. We can also see the maximum number of stages for the 40% yield, configuration 2, is higher than the 40% yield configuration 1, and the maximum number of stages for the 0 dBm input power occurs for a total module gain of 0.005 dB. The reason for the larger number of cascadable stages is that the coupling loss for configuration 2 is lower than that of configuration 1.

For configuration 2 with a 40% yield, there can be about 140 2×2 stages cascaded. In Section III-A, we saw that there can be a 4096×4096 switch network using 2×2 switch modules. In general, an $N \times N$ switching network uses $2 \cdot \log_2 N - 1$. Thus we can see that with 140 stages, an enormous switching network is possible.

2) Maximum Number of Cascadable 4×4 *Switch Modules:* In Fig. 15 we can see the maximum number of 4×4 cascadable switch modules for different device yields. The maximum number of stages is again shown for an input power of 0 dBm to the first stage. For the case of the 20% yield, configuration 1, there is a maximum of 15 stages, and for the 80% yield, there is a maximum of only 2 stages at 0 dBm. Again configuration 2 yields a higher maximum number of stages compared with the same yield for configuration 1. Since the 4×4 switch module losses in the waveguide section are much higher that in the case of the 2×2 switch, the number of stages is greatly decreased.

3) Effect of Filter Bandwidth and Bit Rate on the Maximum Number of Stages: The filter bandwidth and the bit rate both

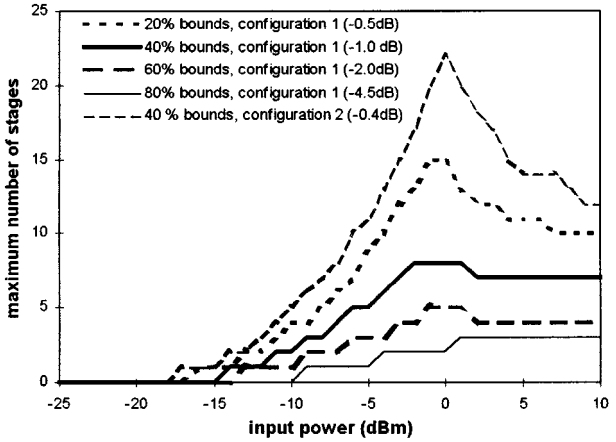

Fig. 15. Maximum number of cascadable 4×4 switch modules for different module yields, as a function of the input power to the switch module.

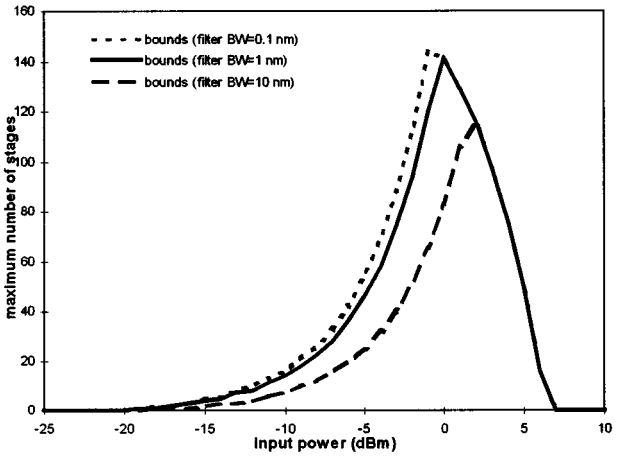

Fig. 16. Effect of the optical filter bandwidth on the maximum number of stages.

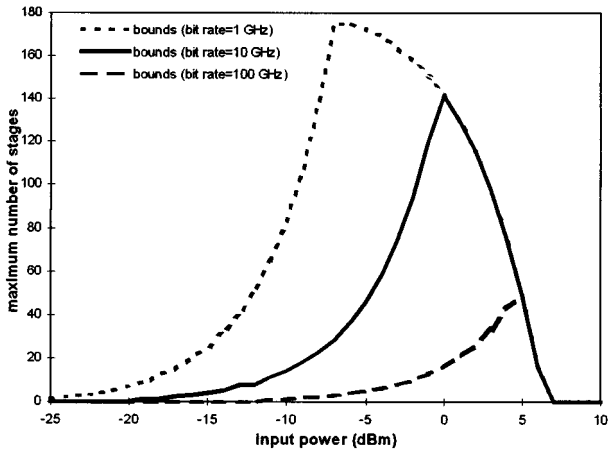

Fig. 17. Effect of bit rate on the maximum number of stages.

effect the maximum number of stages which can be cascaded, since they both effect the BER of the system. As can be seen in Fig. 16, which shows the maximum number of stages for different filter bandwidths, the maximum number of stages increases as the filter bandwidth decreases. The BER decreases as the filter bandwidth decreases since the filter has the effect of limiting the amount of ASE power which makes it to the detector. A smaller optical filter bandwidth filters out more of the ASE. The saturation of the SOA's is not affected, as can be seen from the same bound on the gain saturation limiting side of the curves.

Fig. 17 shows the maximum number of stages for varying bit rates. The maximum number of stages decreases as the bit rate increases, since the BER becomes larger for an increasing bit rate. Again, only the BER is affected, and not the gain saturation of the SOA.

IV. Conclusion

We have shown through a theoretical analysis that it is possible to make a hybrid integrated optical switch using SOA's together with passive polymer waveguides. There can be up to 140 cascadable stages of 2×2 switch modules and 22 4×4 switch modules using configuration 2 for the alignment and attachment of the individual components with a 40% module yield. The 2×2 switch module was found to be the optimum size granularity of the switch module. Using 23 stages of 2×2 switch modules in a Benes architecture, it is possible to make a 4096×4096 switching network. And thus with 140 cascadable stages, a significantly larger switch network is possible.

References

[1] M. Ikeda, "Laser diode switch," *Electron. Lett.*, vol. 17, no. 23, pp. 899–900, 1981.

[2] A. Himeno and M. Kobayashi, "4×4 optical-gate matrix switch," *J. Lightwave Technol.*, vol. LT-3, pp. 230–235, Feb. 1985.

[3] W. Hunziker, "Packaging of optoelectronic components," in *Proc. 2nd Workshop Electroni. LHC Exper.*, Balatonfured, Hungary, Sept. 1996, pp. 365–372.

[4] M. G. Young, U. Koren, B. I. Miller, M. Chien, M. A. Newkirk, and J. M. Verdiell, "A compact 2×2 amplifier switch with integrated DBR lasers operating at 1.55 μm," *IEEE Photon. Technol. Lett.*, vol. 4, pp. 1046–1048, Sept. 1992.

[5] F. Dorgeuille, B. Mersali, M. Feuillade, S. Sainson, S. Slempkès, and M. Foucher, "Novel approach for simple fabrication of high-performance InP-switch matrix based on laser-amplifier gates," *IEEE Photon. Technol. Lett.*, vol. 8, pp. 1178–1180, Sept. 1996.

[6] J. D. Burton, P. J. Fiddyment, M. J. Robertson, and P. Sully, "Monolithic InGaAsP-InP laser amplifier gate switch matrix," *IEEE J. Quantum Electron.*, vol. 29, pp. 2023–2027, June 1993.

[7] M. Janson, L. Lundgren, A.-C. Morner, M. Rask, B. Stoltz, M. Gustavsson, and L. Thylen, "Monolithically integrated 2×2 InGaAsP/InP laser amplifier gate switch arrays," *Electron. Lett.*, vol. 28, no. 8, pp. 776–778, 1992.

[8] C. Holtmann, T. Brenner, R. Dall'Ara, P. A. Besse, and H. Melchior, "Monolithically integrated semiconductor optical amplifiers for transparent 2×2 switches at 1.3 micrometer," *Mitteilungen AGEN*, no. 56–57, pp. 45–48, 1993.

[9] K. Hamamoto and K. Komatsu, "Insertion-loss-free 2×2 InGaAsP/InP optical switch fabricated using bandgap energy controlled selective MOVPE," *Electron. Lett.*, vol. 31, no. 20, pp. 1779–1781.

[10] K. R. Oh, J.-H. Ahn, J. S. Kim, S. W. Lee, H. M. Kim, K. E. Pyun, and H. M. Park, "2×2 InGaAsP/InP laser amplifier gate switch arrays using reactive ion etching," *Electron. Lett.*, vol. 32, no. 1, pp. 39–40.

[11] W. van Berlo, M. Janson, L. Lundgren, A.-C. Morner, J. Terlecki, M. Gustavsson, P. Granestrand, and P. Svensson, "Polarization-insensitive, monolithic 4×4 InGaAsP-InP laser amplifier gate switch matrix," *IEEE Photon. Technol. Lett.*, vol. 7, pp. 1291–1293, Nov. 1996.

[12] E. Almstrom, C. P. Larsen, L. Gillner, W. M. Van Berlo, M. Gustavsson, and E. Berglind, "Experimental and analytical evaluation of packaged 4×4 InGaAsP/InP semiconductor optical amplifier gate switch matrices for optical networks," *J. Lightwave Technol.*, vol. 14, pp. 996–1004, June 1996.

[13] Y. Yamada, H. Terui, Y. Ohmori, M. Yamada, A. Himeno, and M. Kobayashi, "Hybrid-integrated 4×4 optical gate matrix switch using silica-based waveguides and LD array chips," *J. Lightwave Technol.*, vol. 10, pp. 383–389, Mar. 1992.
[14] R. F. Kalman, L. G. Kazovsky, and J. W. Goodman, "Space division switches based on semiconductor optical amplifiers," *IEEE Photon. Technol. Lett.*, vol. 4, pp. 1048–1051, Sept. 1992.
[15] N. A. Olsson, "Lightwave systems with optical amplifiers," *J. Lightwave Technol.*, vol. 7, pp. 1071–1082, July 1989.
[16] M. Ikeda, "Maximum number of connectable laser diode optical switch (LDSW) systems," *Optic. Quantum Electron.*, vol. 20, pp. 515–524, 1988.
[17] L. Gillner and L. Thylén, "Effect of gain saturation in semiconductor laser amplifier links," *IEEE Photon. Technol. Lett.*, vol. 4, pp. 438–441, May 1992.
[18] G. Jeong and J. W. Goodman, "Gain optimization in switches based on semiconductor optical amplifiers," *J. Lightwave Technol.*, vol. 13, pp. 598–605, Apr. 1995.
[19] J. Evankow, Jr. and R. A. Thompson, "Photonic switching modules designed with laser diode amplifiers," *IEEE J. Select. Areas. Commun.*, vol. 6, pp. 1087–1095, Oct. 1988.
[20] S. Yang and J. G. Yao, "Impact of crosstalk induced beat noise on the size of semiconductor laser amplifier based optical space switch structures," *IEEE Photon. Technol. Lett.*, vol. 8, pp. 894–896, July 1996.
[21] E. L. Goldstein, L. Eskildsen, and A. F. Elrefaie, "Performance implications of component crosstalk in transparent lightwave networks," *IEEE Photon. Technol. Lett.*, vol. 6, pp. 657–660, May 1994.
[22] L. Gillner, "Analysis of input power dynamic ranges in two types of expanded semiconductor gate switch arrays," *IEEE Photon. Technol. Lett.*, vol. 8, pp. 536–538, Apr. 1996.
[23] J. Yao and M. O'Mahony, "Impact of input signals on the bit error rate performance of semiconductor-laser-amplifier-based switch systems," *Inst. Elect. Eng. Proc.—Optoelectron.*, vol. 141, no. 4, pp. 265–270, 1994.
[24] R. S. Fan and R. B. Hooker, "Tapered polymer single mode waveguides for mode transformation," *J. Lightwave Technol.*, vol. 17, pp. 466–474, Mar. 1999.
[25] N. Delen and R. B. Hooker, "Free space beam propagation between arbitrarily oriented planes using full diffraction theory: A fast Fourier transform approach," *J. Opt. Soc. Amer. A*, vol. 15, no. 4, 1998.
[26] P. Liao and P. Kelley, *Photonics in Switching, Volume II: Systems*. San Diego, CA: Academic, 1993.
[27] R. C. Steele, G. R. Walker, and N. G. Walker, "Sensitivity of optically preamplified receivers with optical filtering," *IEEE Photon. Technol. Lett.*, vol. 3, pp. 545–547, June 1991.
[28] G. P. Agrawal, *Fiber-Optic Communication Systems*. New York: Wiley, 1992.

Regis S. Fan received the B.S. degree in electrical engineering from the University of Wisconsin, Madison, in 1993 and the M.S. degree in electrical engineering from the University of Colorado, Boulder, in 1995. He received the Ph.D. degree in electrical engineering from the University of Colorado in 1999, where his research focused on optical interconnects using passive optical waveguides and waveguide design.

R. Brian Hooker received the B.A. degree in physics from Brown University, Providence, RI, and the M.S. and Ph.D. degrees in optical sciences from the University of Arizona, Tuscon.

He worked for IBM for nearly 20 years developing technologies and products for optical printing, optical storage, document scanning, and displays. Currently, he is on the Faculty of the University of Colorado, Boulder, where he is engaged in research involving optical interconnects and display systems.